Progress In Electromagnetics Research, PIER 103, 169–184, 2010

PROPERTIES OF DEFECT MODES IN ONE-DIMENSIONAL PHOTONIC CRYSTALS

C.-J. Wu and Z.-H. Wang

Institute of Electro-Optical Science and Technology
National Taiwan Normal University
Taipei 116, Taiwan

Abstract—A theoretical analysis of the properties of the defect modes in a one-dimensional defective photonic crystal (PC) is given. Two defective PCs stacked in symmetric and asymmetric geometries are considered. The defect modes are investigated by the calculated wavelength-dependent transmittance for both TE and TM waves. It is found that there exists a single defect mode within the photonic band gap (PBG) in the asymmetric PC. There are, however, two defect modes within the PBG in the symmetric one. The dependences of defect modes on the angle of incidence are illustrated. Additionally, the effect of defect thickness on the number of defect modes is also examined.

1. INTRODUCTION

A one-dimensional binary dielectric superlattice is a periodic structure that is formed by two distinct dielectrics with different refractive indices. Such a layered structure is usually designed to serve as a dielectric mirror (also known as a Bragg reflector) which plays an important part in many modern photonic systems [1–4]. A periodic bilayer system is now known as one-dimensional photonic crystal (1DPC), which has been a hot topic in optical physics over the past two decades [5–16]. In a PC, there will be photonic band gaps (PBGs) created due to the spatial periodicity.

By capitalizing on the existence of the PBGs in a PC, one of the important and useful applications in photonics is to utilize the PBG to design a multilayer narrowband transmission filter also called a Fabry-Perot resonator (FPR). An FPR can be simply realized by introducing a defect layer into the PC to break the spatial periodicity. This defect

Corresponding author: Z.-H. Wang (abcd5855tw@yahoo.com.tw).

layer behaves, in principle, as a cavity resonator when the resonant condition is satisfied. The defect modes will be located within the PBG, which are much similar to the defect states generated in the forbidden band in a doped semiconductor. Materials for the defect layer usually call for dielectrics [1–4]. Recently, due to the realization of a metamaterial with negative refractive index (NRI) predicted by Veselago [17], defect layer using NRI materials are also available [18–20]. In addition, by making use of an electro-optical nonlinear defect, the device can become tunable [21–24].

In a 1DPC, adding a defect layer D in it will lead to the system denoted as $A/(HL)^N D(HL)^N/S$ where A means the usual air, N is the number of periods for the periodic bilayers, and S denotes the substrate. In addition, H and L are the high- and low-index layers with their thicknesses usually set to be quarter-wavelength, i.e., $n_H d_H = n_L d_L = \lambda_0/4$, where n_H, n_L, and d_H, d_L are the refractive indices and thicknesses of H and L, respectively, and λ_0 is the design wavelength. The above structure is referred to as an asymmetric defective PC with respect to the defect layer D, as depicted in the lower one of Fig. 1. In addition to the asymmetric structure, the defective PC can also be designed in a symmetric manner like $A/(HL)^N D(LH)^N/S$, as depicted in the upper one of Fig. 1.

The purpose of this paper is to investigate the properties of defect modes in these two defective PCs. We specifically investigate the defect modes as a function of the angle of incidence for both TE and TM waves for both the symmetric and asymmetric defective PCs. As we shall show later, in the asymmetric PC, we find there is only one defect

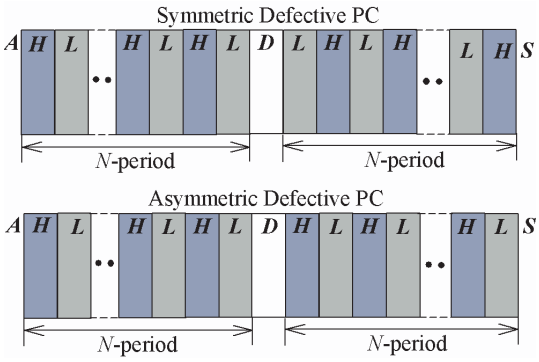

Figure 1. Structures of two defective PCs, in which the upper one is referred to as symmetric PC, whereas the asymmetric one is depicted in the lower figure.

mode within the PBG. However, there will be two defect modes in the symmetric PC. The presence of two defect modes may be more efficient in utilizing the PBG compared to the single mode in the asymmetric one [25, 26]. Moreover, the feature of two-mode makes the structure more useful in the signal processing especially in optical communication. For instance, it can be used as a frequency-selective filter (or wavelength multiplexer) that can extract two signals with fairly different frequencies. The analysis on the properties of defect modes gives some useful information for the design of narrowband transmission filter based on the one-dimensional PCs.

2. THEORY

Let us first consider the symmetric defective PC with a structure of $A/(HL)^N D(LH)^N/S$, as depicted in Fig. 1. The transmittance T is related to the transmission coefficient t by

$$T = \frac{n_S \cos\theta_S}{n_A \cos\theta_A}|t|^2, \tag{1}$$

where t is given by

$$t = \frac{1}{M_{11}}, \tag{2}$$

according to the transfer matrix method [2], where M_{11} is one of the matrix elements of the total system matrix $\mathbf{M}$ written by

$$\mathbf{M} = \begin{pmatrix} M_{11} & M_{12} \\ M_{21} & M_{22} \end{pmatrix}. \tag{3}$$

The total system matrix is given by

$$\begin{aligned} \mathbf{M}_{sym} \;=\; & \mathbf{D}_A^{-1}\left[\mathbf{D}_H\mathbf{P}_H\mathbf{D}_H^{-1}\mathbf{D}_L\mathbf{P}_L\mathbf{D}_L^{-1}\right]^N\left[\mathbf{D}_D\mathbf{P}_D\mathbf{D}_D^{-1}\right] \\ & \left[\mathbf{D}_L\mathbf{P}_L\mathbf{D}_L^{-1}\mathbf{D}_H\mathbf{P}_H\mathbf{D}_H^{-1}\right]^N\mathbf{D}_S, \end{aligned} \tag{4}$$

where the dynamical matrix in Eq. (4) for medium i is given by

$$\mathbf{D}_i = \begin{pmatrix} 1 & 1 \\ n_i\cos\theta_i & -n_i\cos\theta_i \end{pmatrix}, \tag{5}$$

for TE wave and

$$\mathbf{D}_i = \begin{pmatrix} \cos\theta_i & \cos\theta_i \\ n_i & -n_i \end{pmatrix}, \tag{6}$$

for TM wave, and $i = A$, H, L, and S, respectively. The translational matrix in layer H, L, or D is expressed as

$$\mathbf{P}_i = \begin{pmatrix} \exp(j\phi_i) & 0 \\ 0 & \exp(-j\phi_i) \end{pmatrix}, \tag{7}$$

where the phase is $\phi_i = 2\pi n_i d_i/\lambda$, where λ is the wavelength of the incident wave. In the above formulations, n_i, θ_i, and d_i are the refractive index, the ray angle, and the thickness of layer i, respectively. For $i = A$, the ray angle in air is then equal to the incident angle denoted by $\theta \equiv \theta_A$. All the ray angles are related by the Snell's law of refraction.

As for the asymmetric defective PC shown in the bottom of Fig. 1, the total system matrix is given by

$$\mathbf{M}_{asy} = \mathbf{D}_A^{-1}\left[\mathbf{D}_H\mathbf{P}_H\mathbf{D}_H^{-1}\mathbf{D}_L\mathbf{P}_L\mathbf{D}_L^{-1}\right]^N\left[\mathbf{D}_D\mathbf{P}_D\mathbf{D}_D^{-1}\right] \left[\mathbf{D}_H\mathbf{P}_H\mathbf{D}_H^{-1}\mathbf{D}_L\mathbf{P}_L\mathbf{D}_L^{-1}\right]^N\mathbf{D}_S. \quad (8)$$

From Eq. (8), we can obtain the matrix element M_{11}, the transmittance T in this case is determined again by Eqs. (1) and (2).

3. NUMERICAL RESULTS AND DISCUSSION

In what follows we shall investigate the defect modes based on the calculated angle-dependent transmittance for both the asymmetric and symmetric defective PCs. The material parameters used in our calculation are $n_H = 2.1$ for layer H, $n_L = n_D = 1.4$ for layer L and D. Without loss of generality, the defect modes are investigated for the quarter-wavelength stack, i.e., $n_H d_H = n_L d_L = \lambda_0/4$ with a design wavelength of $\lambda_0 = 1550\,\text{nm}$ in infrared region. We choose the quarter-wavelength stack because its analytical expression for the transmittance can be obtained and thus some physics can be gained insight directly. In addition, we choose $\lambda_0 = 1550\,\text{nm}$ for its use in optical communications. The number of periods for each PC is $N = 10$. The substrate S is simply assumed to be air with $n_S = n_A = 1$.

3.1. Defect Modes in Asymmetric PC A/(HL)^{10}L(HL)^{10}/S

In Fig. 2, we have plotted the wavelength-dependent transmittance for the asymmetric PC in TE wave at different angles of incidence 0°, 15°, 30°, 45°, 60°, and 75°, respectively. Some features are of note. In this case, there is a single resonant peak within the PBG which corresponds to the so-called defect mode. For normal incidence, i.e., at 0°, it is seen that this resonant peak locates at the design wavelength of $\lambda_0 = 1550\,\text{nm}$. The peak height is then strongly decreased with the increase in the angle of incidence. At a much larger angle, say 75°, the resonant peak height has been lowered down to 0.16. In addition, the position of defect mode is shifted to the left as the angle of incidence increases. The decrease in peak height means an incomplete resonance at the defect mode.

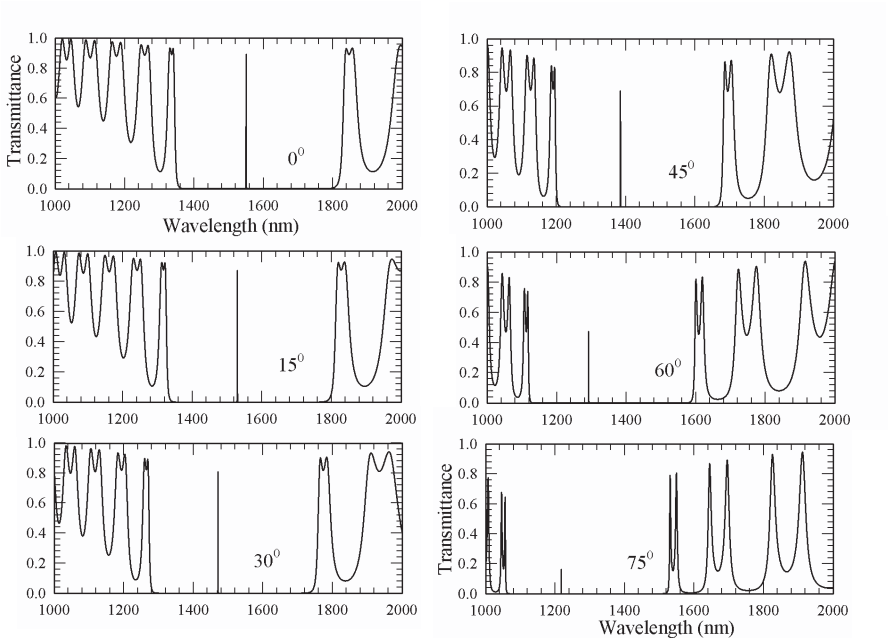

Figure 2. Calculated TE-wave transmittance for the asymmetric filter $A/(HL)^{10}L(HL)^{10}/S$ as a function of the wavelength at different angles of incidence 0°, 15°, 30°, 45°, 60°, and 75°, respectively.

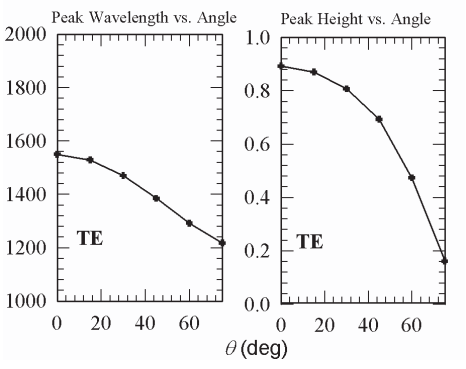

Figure 3. The angle-dependent peak wavelength (left) and peak height (right) for the defect mode in asymmetric filter $A/(HL)^{10}L(HL)^{10}/S$ in TE wave.

Another feature in Fig. 2 that is worth mentioning is the width of PBG. In normal incidence, the left band edge λ_L and right band edge λ_R can be analytically determined by the theory of Bragg reflector, i.e., they can be obtained by using the following equation [1],

$$\lambda_L = \frac{\pi\left(n_H d_H + n_L d_L\right)}{\cos^{-1}\left(-\rho\right)}, \quad \lambda_R = \frac{\pi\left(n_H d_H + n_L d_L\right)}{\cos^{-1}\left(\rho\right)}, \tag{9}$$

where $\rho = (n_H - n_L)/(n_H + n_L)$ is the Fresnel coefficient. Based on Eq. (9) together with the given material parameters, the calculated band edges are given by $\lambda_L = 1374\,\text{nm}$ and $\lambda_R = 1778\,\text{nm}$. The band gap has a size of 404 nm with band center λ_c at 1556 nm. Good agreement with the Fig. 2 is thus seen. As the incident angle increases, both λ_L and λ_R moved to the left. As a result, the PBG is moved to the left, as illustrated in Fig. 2. The dependence of peak wavelength and peak height on the angle of incidence is plotted in Fig. 3.

The defect modes for TM wave are plotted in Fig. 4, in which the angles of incidence 0°, 15°, 30°, 45°, 60°, and 75° in Fig. 2 are also taken

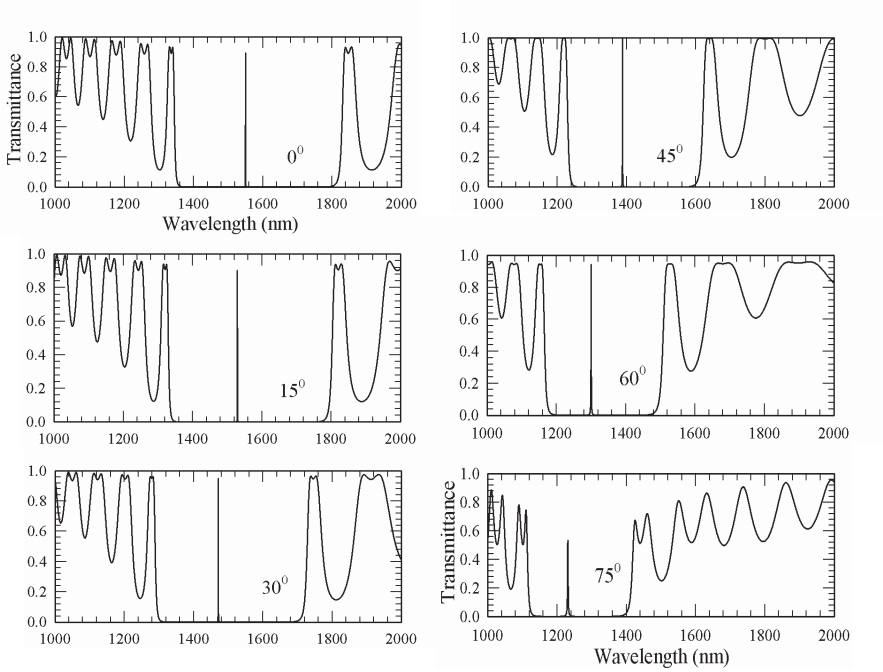

Figure 4. Calculated TM-wave transmittance for the asymmetric filter $A/(HL)^{10}L(HL)^{10}/S$ as a function of the wavelength at different angles of incidence 0°, 15°, 30°, 45°, 60°, and 75°, respectively.

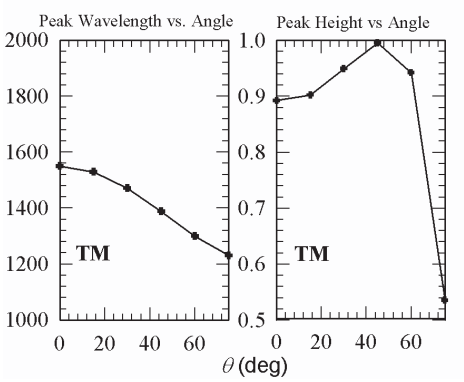

Figure 5. The angle-dependent peak wavelength (left) and peak height (right) for the defect mode in asymmetric filter $A/(HL)^{10}L(HL)^{10}/S$ in TM wave.

for the purpose of comparison. For normal incidence, i.e., at 0°, the figure is identical to that in Fig. 2 because there is no difference between TE and TM waves at normal incidence. Like in TE wave, the position of defect mode is shifted to shorter wavelength as the angle increases. The resonant peak height is initially increases appreciably from 0° to 45° and then decreases as the angle increases. The dependence of peak wavelength and peak height on the incident angle in this case is shown in Fig. 5.

To explain the above properties in the asymmetric defective PC, let us start from the simple normal incidence. In this case, an exact expression for the transmittance at design wavelength can be found, namely

$$T(\lambda_0) = \frac{4}{\left[\left(\frac{n_L}{n_H}\right)^{2N} + \left(\frac{n_H}{n_L}\right)^{2N}\right]^2 \cos^2\left(\frac{2\pi}{\lambda_0} n_D d_D\right) + \left(n_D + \frac{1}{n_D}\right)^2 \sin^2\left(\frac{2\pi}{\lambda_0} n_D d_D\right)}. \quad (10)$$

With the fact that

$$n_D d_D = n_L d_L = \frac{\lambda_0}{4}, \quad (11)$$

and thus $\cos(2\pi n_D d_D/\lambda_0) = 0$ and $\sin(2\pi n_D d_D/\lambda_0) = 1$, it can be seen from Eq. (10) that there will be a single defect mode at λ_0 with a maximum transmittance,

$$T(\lambda_0) = \frac{4}{\left(n_D + \frac{1}{n_D}\right)^2}. \quad (12)$$

The peak height will thus be lowered down as n_D increases. That explains why we chose the low-index layer as a defect. Now with $n_D = 1.4$, Eq. (12) yields $T(\lambda_0) = 0.895$ consistent with the results shown in the top curves of Figs. 2 and 4, and the right curves of Figs. 3 and 5. It should be noted that the peak transmittance can be unity if the defect layer is replaced by the air of $n_D = 1$. In addition, Eq. (12) shows that the peak height and the peak wavelength are independent of the stack number N. The effects of N are to narrow the peak shape and to make the band edges more sharp as N increases.

Physically, the presence of a single defect mode can be understood by making use of the equivalent absentee layer, i.e., two consecutive quarter-wavelength layers of HH or LL will effectively reduce to be absentee. Thus, the asymmetric filter can be equivalently reduced to a single quarter-wavelength layer as follows:

$$\begin{aligned}(HL)^N L(HL)^N &\rightarrow (HL)^{N-1} HLLHL(HL)^{N-1} \\ &\rightarrow (HL)^{N-1} L(HL)^{N-1} \rightarrow \cdots \rightarrow L. \end{aligned} \tag{13}$$

For a single quarter-wavelength layer, it can be regarded as a simple single-layer FPR with the transmittance peak occurring when the optical length L_p is given by

$$L_p = n_D d_D = n_L d_L = \frac{\lambda_0}{4}(2m+1), \quad m = 0, 1, 2, \ldots. \tag{14}$$

For $m = 0$, Eq. (14) leads to Eq. (11). The origin of single defect mode is thus seen.

Now let us continue to investigate the angular dependence of defect mode. At resonance, the multilayer effectively acts a single layer and the resonance condition in Eq. (11) or (14), in the oblique incidence, should be corrected as

$$L_p = n_D d_D \cos\theta_D = n_L d_L \cos\theta_L = \frac{\lambda_0}{4}\cos\theta_L, . \tag{15}$$

The peak position is proportional to $\cos\theta_L$. Thus, the peak wavelength will be less than λ_0 and decrease with the increase in the incident angle θ_A because

$$\cos\theta_L = \sqrt{1 - \frac{n_A^2}{n_L^2}\sin\theta_A}. \tag{16}$$

This explains the shifting properties as the incident angle increases, as illustrated in Fig. 2 for TE wave and 4 for TM wave, respectively.

As for the angle-dependent peak height, we can physically understand as follows: Again, at resonance, we treat the structure as a single defect slab. For a slab under oblique, in TE wave, it is known that the reflectance is an increasing function of the incident

angle, which means the transmittance will decrease as the angle increases. Thus the transmittance peak height will decrease as a function of the incident angle, as shown in Fig. 2 and the right in Fig. 3, respectively. However, in TM wave, it is known that there exists the Brewster angle (at which transmittance is unity) in the angle-dependent transmittance. For the angles smaller than Brewster angle, the transmittance is an increasing function and then becomes a decreasing function when the angle larger than the Brewster angle. Such properties are evidently illustrated in Fig. 4 and the right in Fig. 5, respectively. In addition, we have found an effective Brewster angle $\sim 45^\circ$ in TM wave in this filter.

3.2. Defect Modes in Symmetric PC $A/(HL)^{10}L(LH)^{10}/S$

In Fig. 6, we have plotted the wavelength-dependent transmittance for the symmetric PC in TE wave at different angles of incidence, 0°, 15°, 30°, 45°, 60°, and 75°, respectively. In this case, there are two defect modes, as indicated by the two resonant peaks 1 and 2 within

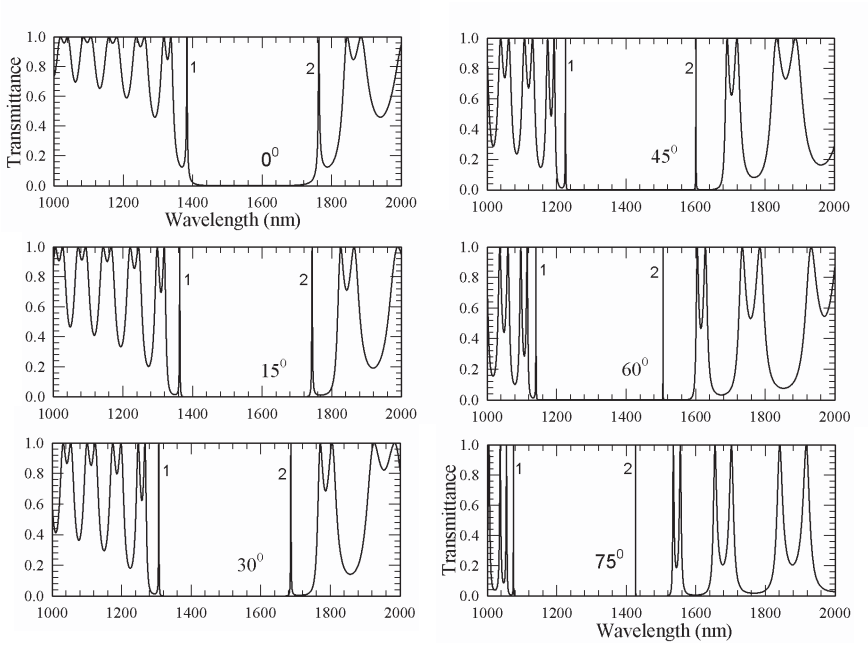

Figure 6. Calculated TE-wave transmittance the symmetric filter $A/(HL)^{10}L(LH)^{10}/S$ as a function of the wavelength at different angles of incidence 0°, 15°, 30°, 45°, 60°, and 75°, respectively.

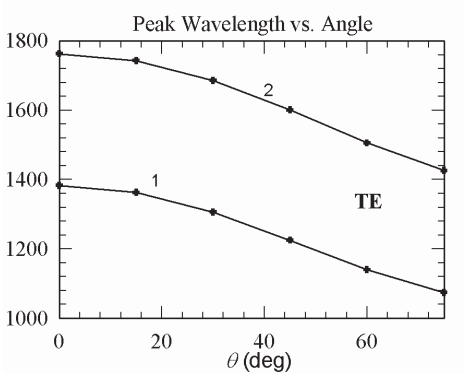

Figure 7. The angle-dependent two peak wavelengths for the defect mode in symmetric filter $A/(HL)^{10}L(LH)^{10}/S$ in TE wave.

the PBG. The presence of two defect modes can be ascribed to the structural reflection symmetry [27]. This feature of symmetry will give rise to two possible field solutions in the defect layer at resonance. One solution proportional to cosine function belongs to an even symmetry which corresponds to the lower energy state, as marked by 2. The other proportional to sine function is an odd symmetry and is indicated by 1. The dependence of defect modes 1 and 2 on the angle of incidence is plotted in Fig. 7.

For normal incidence, $\theta = 0°$, we see that the left peak locates at the wavelength less than the design wavelength λ_0 whereas the position of right peak is higher than λ_0. If the incident angle increases, then, similar to the asymmetric case, the positions of two defect modes are again shifted to the left. However, the peak heights for the two peaks remain unchanged as the incident angle changes.

Shown in Fig. 8 are the defect modes in TM wave for the symmetric PC. The peak heights of two defect modes, the same as in Fig. 6, are not influenced by the incident angle. The positions of two defect modes are also moved to shorter wavelength as the incident angle increases. Moreover, the separation of two peaks is decreased with the increase in the angle of incidence. The positions of two defect modes as a function of the angle of incidence are shown in Fig. 9.

To explain the above properties in the symmetric defective PC, we again start from the simple normal incidence. In this case, an explicit expression for the transmittance at design wavelength can be found to

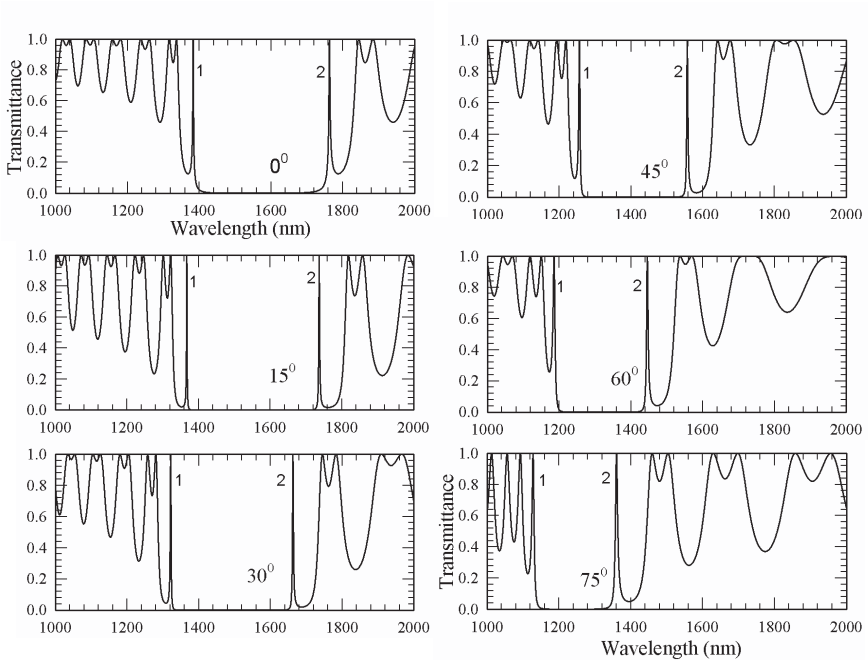

Figure 8. Calculated TM-wave transmittance symmetric PC $A/(HL)^{10}L(LH)^{10}/S$ as a function of the wavelength at different angles of incidence 0°, 15°, 30°, 45°, 60°, and 75°, respectively.

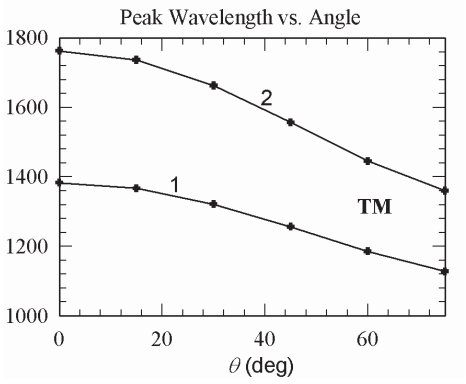

Figure 9. The peak wavelength for the defect mode in symmetric PC $A/(HL)^{10}L(LH)^{10}/S$ in TM wave as a function of angle of incidence.

be

$$T(\lambda_0) = \frac{4}{4\cos^2\left(\frac{2\pi}{\lambda_0} n_D d_D\right) + \left[\frac{1}{n_D}\left(\frac{n_L}{n_H}\right)^{2N} + n_D\left(\frac{n_H}{n_L}\right)^{2N}\right]^2 \sin^2\left(\frac{2\pi}{\lambda_0} n_D d_D\right)}. \quad (17)$$

With $n_D d_D = n_L d_L = \lambda_0/4$, Eq. (17) becomes

$$T(\lambda_0) = \frac{4}{\left[\frac{1}{n_D}\left(\frac{n_L}{n_H}\right)^{2N} + n_D\left(\frac{n_H}{n_L}\right)^{2N}\right]^2} \approx \frac{4}{\left[n_D\left(\frac{n_H}{n_L}\right)^{2N}\right]^2}, \quad (18)$$

which is obviously very close to zero as $N \gg 1$. It is concluded that there will be no defect mode at the design wavelength $\lambda_0 = 1550\,\text{nm}$ in this case, as illustrated in the top curve of Fig. 6. In fact, numerical results demonstrate that there are two defect modes away from λ_0.

The presence of two defect modes can be qualitatively explained as follows: Due to the structurally reflection symmetry, the structure can be analogously regarded as a single attractive quantum well when resonance occurs. In a single quantum well, it is known that there will two kinds of bound states that could be even and odd symmetry in wavefunctions. The even symmetry means the wavefunction is proportional to cosine function, while it is proportional to sine function for the odd symmetry. The even bound state equivalently corresponds to defect mode 2 (in Fig. 8) with lower energy whereas the odd bound state with a higher energy corresponds to the defect mode 1.

As for the angular dependence of the peak positions, we can similarly use Eqs. (15) and (16) to reason the shifting behaviors in the defect modes. In this symmetric one, the two defect modes has a complete transmission, i.e., $T = 1$, which can be ascribed to the impedance match when resonates. Impedance match means the whole structure is matched to the air such that the reflection coefficient is zero.

3.3. Thickness Effect in Asymmetric PC $A/(HL)^{10}mL(HL)^{10}/S$

Let us finally examine the effect of defect thickness on the number of defect modes in asymmetric defective PC, $A/(HL)^{10}mL(HL)^{10}/S$, where m representing the repeated number of defect layer is limited to the condition of $m < 10$. Some results in normal incidence are shown in Fig. 10, where the left is plotted at $m =$ odd and the right is for $m =$ even. It is of interest to see that the number of defect modes is odd when m is odd, and is even when m is even. For the odd number of $m = 1$ (See Figs. 2 and 4), 3, 5, and 7, there is always a single defect

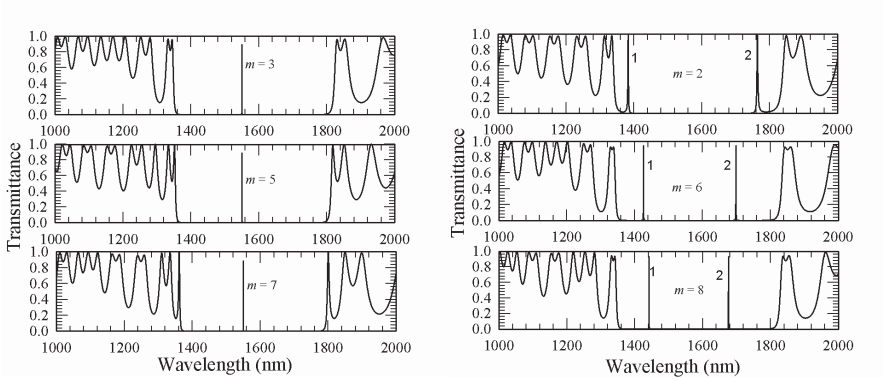

Figure 10. The transmittance spectra in asymmetric PC $A/(HL)^{10}mL(HL)^{10}/S$ in normal incidence at different numbers of defect layers, m = odd (left) and m = even (right).

mode fixed at 1550 nm. This dependence can be simply understood by using absentee layer, that is, $mL \rightarrow L$, for m = odd. The structure thus effectively has a single defect L as described previously.

For m = even, in Fig. 10, two defect modes appear with the PBG. In addition, the separation of these two defect modes decreases as m increases. The appearance of two defect modes can be qualitatively explained as follows. For m = even, the structure $(HL)^N mL(HL)^N$ is identical to $H(LH)^{N-1}(m+1)L(HL)^N$, which can be approximately as a symmetric one with defect layer of $(m+1)L$ if N is large. Based on the previous discussion in the symmetrical filter, it is thus expected to have two defect modes in this case.

The presence of multiple defect modes at the even number of m makes the structure possible to be designed as a multichannel filter which can efficiently enhance the spectral utilization in the PBG instead of using the quantum-well defect [26, 28].

4. CONCLUSION

Based on the calculated resonant transmission properties in a defective 1DPC, the properties of the defect modes for the asymmetric and symmetric structures have been theoretically investigated. In an asymmetric structure, there is a single defect mode inside the PBG. The peak height is strongly dependent on the angle of incidence for both TE and TM waves. The position of defect mode moves to shorter wavelength as the angle increases. In a symmetric one, we

find that there are two defect modes. The peak heights of these two modes are independent of the incident angle. The effect of the incident angle is to shift the defect positions to the shorter wavelengths. The dependence of defect thickness on the number of defect modes is also illustrated. The analysis on the defect modes provides useful information for the design of a narrowband transmission filter based on the 1DPCs. Finally, it is worthwhile to mention that the local defect modes in this study are mainly due to the presence of defect layer in the structure. However, the other possible local defects arising from the external surfaces are beyond the current work.

ACKNOWLEDGMENT

C.-J. Wu acknowledges the financial support from the National Science Council of the Republic of China under Contract No. NSC-97-2112-M-003-013-MY3.

REFERENCES

1. Orfanidis, S. J., *Electromagnetic Waves and Antennas*, Chapter 7, Rutger University, 2008, www.ece.rutgers.edu/∼orfanidi/ewa.
2. Yeh, P., *Optical Waves in Layered Media*, John Wiley & Sons, Singapore, 1991.
3. Born, M. and E. Wolf, *Principles of Optics*, Cambridge, London, 1999.
4. Hecht, E., *Optics*, Chapter 9, Addison Wesley, New York, 2002.
5. Yablonovitch, E., "Inhibited spontaneous emission in solid state physics and electronics," *Phys. Rev. Lett.*, Vol. 58, 2059–2062, 1987.
6. John, S., "Strong localization of photons in certain disordered lattices," *Phys. Rev. Lett.*, Vol. 58, 2486–2489, 1987.
7. Joannopoulos, J. D., R. D. Meade, and J. N. Winn, *Photonic Crystals: Molding the Flow of Light*, Princeton University Press, Princeton, NJ, 1995.
8. Yariv, A. and P. Yeh, *Photonics*, Oxford University Press, New York, 2007.
9. Srivastava, R., K. B. Thapa, S. Pati, and S. P. Ojha, "Omni-direction reflection in one dimensional photonic crystal," *Progress In Electromagnetics Research B*, Vol. 7, 133–143, 2008.
10. Srivastava, R., S. Pati, and S. P. Ojha, "Enhancement of

omnidirectional reflection in photonic crystal heterostructures," *Progress In Electromagnetics Research B*, Vol. 1, 197–208, 2008.

11. Awasthi, S. K., U. Malaviya, S. P. Ojha, N. K. Mishra, and B. Singh, "Design of a tunable polarizer using a one-dimensional nano sized photonic bandgap structure," *Progress In Electromagnetics Research B*, Vol. 5, 133–152, 2008.
12. Golmohammadi, S., Y. Rouhani, K. Abbasian, and A. Rostami, "Photonic bandgaps in quasiperiodic multilayer using Fourier transform of the refractive index profile," *Progress In Electromagnetics Research B*, Vol. 18, 311–325, 2009.
13. Banerjee, A., "Tunable polarizer using a one-dimensional nano sized photonic bandgap structure," *Progress In Electromagnetics Research B*, Vol. 5, 133–152, 2008.
14. Banerjee, A., "Enhanced temperature sensing by using one-dimensional ternary photonic band gap structures," *Progress In Electromagnetics Research Letters*, Vol. 11, 129–137, 2009.
15. Wu, C.-J., B.-H. Chu, M.-T. Weng, and H.-L. Lee, "Enhancement of bandwidth in a chirped quarter-wave dielectric mirror," *Journal of Electromagnetic Waves and Applications*, Vol. 23, No. 4, 437–447, 2009.
16. Wu, C.-J., B.-H. Chu, and M.-T. Weng, "Analysis of optical reflection in a chirped distributed Bragg reflector," *Journal of Electromagnetic Waves and Applications*, Vol. 23, No. 1, 129–138, 2009.
17. Veselago, V. G., "The electrodynamics of substances with simultaneously negative values of permittivity and permeability," *Sov. Phys. Usp.*, Vol. 10, 509–514, 1968.
18. Hsu, H.-T. and C.-J. Wu, "Design rules for a Fabry-Perot narrow band transmission filter containing a metamaterial negative-index defect," *Progress In Electromagnetics Research Letters*, Vol. 9, 101–107, 2009.
19. Wang, Z.-Y., X.-M. Cheng, X.-Q. He, S.-L. Fan, and W.-Z. Yan, "Photonic crystal narrow filters with negative refractive index structural defects," *Progress In Electromagnetics Research*, PIER 80, 421–430, 2008.
20. Boedecker, G. and C. Henkle, "All-frequency effective medium theory of a photonic crystal," *Optics Express*, Vol. 13, 1590–1595, 2003.
21. Ha, Y. K., Y. C. Yang, J. E. Kim, and H. Y. Park, "Tunable omnidirectional reflection bands and defect modes of a one-dimensional photonic band gap structure with liquid crystals,"

Appl. Phys. Lett., Vol. 79, 15–17, 2001.

22. Lu, Y. Q. and J. J. Zheng, "Frequency tuning of optical parametric generator in periodically poled optical superlattice $LiNbO_3$ by electro-optic effect," *Appl. Phys. Lett.*, Vol. 74, 123–125, 1999.
23. Zhu, Q. and Y. Zhang, "Defect modes and wavelength tuning of one-dimensional photonic crystal with lithium niobate," *Optik*, Vol. 120, 195–198, 2009.
24. Wu, C.-J., J.-J. Liao, and T. W. Chang, "Tunable multilayer Fabry-Perot resonator using electro-optical defect layer," *Journal of Electromagnetic Waves and Applications*, Vol. 24, 531–542, 2010.
25. Hu, X., Q. Gong, S. Feng, B. Cheng, and D. Zhang, "Tunable multichannel filter in nonlinear ferroelectric photonic crystal," *Optics Communication*, Vol. 253, 138–144, 2005.
26. Liu, J., J. Sun, C. Huang, W. Hu, and D. Huang, "Optimizing the spectral efficiency of photonic quantum well structures," *Optik*, Vol. 120, 35–39, 2009.
27. Smith, D. R., R. Dalichaouch, N. Kroll, S. Schultz, S. L. McCall, and P. M. Platzman, "Photonic band structure without and with defect in one-dimensional photonic crystal," *J. Opt. Soc. Am. B: Optical Physics*, Vol. 10, 314–321, 1993.
28. Qiao, F., C. Zhang, and J. Wan, "Photonic quantum-well structure: Multiple channeled filtering phenomena," *Appl. Phys. Lett.*, Vol. 77, 3698–3700, 2000.